Journal of Catalysis **191,** 261–270 (2000)
doi:10.1006/jcat.1999.2797, available online at http://www.idealibrary.com on IDEAL®

Mass-Transfer Limitation in Mesopores of Ni–MgO Catalyst in Liquid-Phase Hydrogenation

Satoshi Sato,*[,1] Ryoji Takahashi,* Toshiaki Sodesawa,* Fumio Nozaki,* Xing-Zhou Jin,† Satoshi Suzuki,† and Tomohiro Nakayama†

*Department of Applied Chemistry, Faculty of Engineering, and †Graduate School of Science and Technology, Chiba University, Yayoi, Inage, Chiba 263-8522, Japan

Received April 7, 1999; revised October 21, 1999; accepted November 5, 1999

Liquid-phase hydrogenation of cyclohexanone, acetone, 2-butanone, 3-pentanone, and 4-heptanone to the corresponding secondary alcohols was investigated over various porous Ni catalysts at 0°C under a hydrogen pressure of 1.1 MPa. Pore size distributions as well as Ni surface area of Ni–MgO catalysts, which were prepared from a melt of the corresponding nitrates and citric acid, with high Ni contents of 60–80 wt% were controlled by the calcination temperature of the precursors. For the hydrogenation of acetone, reaction rate constants were directly proportional to the Ni surface areas of the catalysts, and Raney nickel which had the largest Ni surface area showed the highest reaction rate. For the hydrogenation of other reactants larger than acetone in molecular size, however, rate constants do not have a simple linear correlation with Ni surface area. Ni–MgO catalysts with large mesopores exhibited reaction rates higher than those of Raney nickel catalysts with the largest Ni surface areas. Assuming that diffusion of both reactants and products is restricted in small pores such as in Raney nickel, we tried to evaluate an effective pore size for the liquid-phase mass transfer in porous materials by a novel approach analyzing reaction rate data coupled with pore size distribution and hydrogen chemisorption data. Cumulative Ni surface areas were calculated by multiplying the Ni surface area by a fraction of cumulative surface area located in pores larger than a specific size to the total surface area, and relationship between the cumulative Ni surface areas and the reaction rate constants were examined. It was found that the rate constants for the hydrogenation of 2-butanone, cyclohexanone, 3-pentanone, and 4-heptanone were proportional to cumulative Ni surface areas in pores larger than critical sizes of 2.0, 2.3, 3.2, and 3.7 nm in radius, respectively. It has been consequently elucidated that the mass transfer of the reactants is restricted in pores smaller than a critical size that depends on the size of the reactants.

Key Words: **Ni–MgO; citric acid; hydrogenation; cyclohexanone; acetone; 2-butanone; 3-pentanone; 4-heptanone; mass-transfer limitation; liquid phase.**

INTRODUCTION

Group VIII metals such as Pt, Pd, Ru, Rh, Ir, Os, Co, and Ni have been used in catalytic hydrogenation of olefins and carbonyl compounds in organic syntheses (1). The metal catalysts are prepared in the form of not only metal particles dispersed on supporting materials but also porous bulk metals. Porous metals such as Raney nickel and Raney cobalt prepared by dissolution of Al from Ni–Al and Co–Al alloy are frequently used as catalysts for liquid-phase hydrogenation (1–7). Reduced fine nickel powders are also effective as bulk metals for catalytic hydrogenation (8, 9).

We have recently reported that Ni–MgO catalysts, which are prepared using a melt of nickel nitrate, magnesium nitrate, and citric acid, have high nickel metal surface areas and efficient catalytic activities for several gas-phase reactions (10, 11). In our preliminary work (12), we have applied the Ni–MgO catalyst with high Ni surface area to the liquid-phase hydrogenation of cyclohexanone to cyclohexanol, and found that the Ni–MgO catalysts with high Ni contents ranging from 60 to 80 wt% exhibited reaction rates higher than those of Raney nickel catalysts, which had pores smaller than those of the Ni–MgO. In addition, it has been reported that hydrogenation rate in the liquid phase sometimes has no correlation with metal surface area of Raney nickel (13). We have speculated that the diffusion of reactants and/or products in the mesopore region probably causes the reaction rate.

Even in the vapor phase, diffusion processes of reactants in micropores of zeolites are well known to be restricted (14, 15). In the liquid phase, resistance to mass transfer is often large enough to compete with surface reaction. In some cases, the liquid-phase hydrogenation rate is slower than the vapor-phase hydrogenation rate (16). The mass-transfer resistance reduces the effectiveness of the catalyst (17–19). Interparticle mass transfer resistance can be eliminated by increasing stirring speed in a batch reactor, and pore diffusion can be evaluated by using catalysts with different particle sizes (19). Actually, the reaction rates in

[1] To whom correspondence should be addressed. E-mail: satoshi@planet.tc.chiba-u.ac.jp.

0021-9517/00 $35.00

the acetone hydrogenation depend on the particle size of the Raney Ni catalyst (20). Thus, we examine a novel approach to identify sizes of pore in which reactants can diffuse with negligible mass-transfer resistance by analyzing reaction rate data coupled with pore size distribution and hydrogen chemisorption data.

In this work, we first examine the influence of calcination temperature on the pore structure and Ni surface area of Ni–MgO catalysts. Second, as an attempt to clarify the liquid-phase mass-transfer limitation of reactants in the mesopores of Ni catalysts, we examine the liquid-phase hydrogenation of cyclohexanone, comparing it with the behavior of Raney nickel catalyst. We found a definite correlation between the reaction rate constant and the cumulative Ni surface area of pores higher than a particular size, analyzing the reaction rate data coupled with pore size distribution and Ni surface area. Third, we examine the new approach to the hydrogenations of several reactants such as acetone, 2-butanone, 3-pentanone, and 4-heptanone. We propose a convincing argument on the mass-transfer limitation in the mesopores of catalysts for liquid-phase hydrogenation.

EXPERIMENTAL

Catalyst Preparation

NiO–MgO samples with different nickel contents were prepared according to the procedure described elsewhere (10, 11). An amorphous mixture of citrates of Ni and Mg was calcined at temperatures ranging from 250 to 550°C. Prior to the catalytic tests and the characterization of catalysts, the NiO–MgO powder sample (0.1 g) was reduced in a glass tube vessel (volume, 50 cm^3; length, 146 mm; o.d., 21 mm) under hydrogen flow (80 mmol h^{-1}) at 500°C for 2 h. During the reduction, the glass vessel was connected to a silicone plug through which two glass pipes passed; one pipe is for inlet of hydrogen flow and the other is for outlet. After the reduced sample had been cooled to room temperature, the glass vessel with the freshly reduced sample served for the following hydrogenation reaction, being placed into a pressure batch reactor.

Reference Raney Ni catalysts were prepared by leaching Al from commercial Ni–Al alloy (40 and 50 wt% Ni, Wako Chemical, Ltd.) with NaOH aqueous solution at 50°C [Method II in Ref. (21)]. The Raney Ni catalysts prepared from commercial Ni–Al alloy containing 40 and 50 wt% Ni are hereafter abbreviated Raney 40 and Raney 50, respectively. About 0.1 g of Raney nickel freshly prepared from 0.20–0.25 g of the Ni–Al alloy in the glass vessel was supplied to the following reaction, after it had been washed with ethanol and *n*-hexane, each twice.

Characterization of Catalyst

Specific surface areas of the samples were determined by the BET method using the nitrogen adsorption isotherm at −196°C in a conventional volumetric gas adsorption apparatus. A pore size distribution was calculated using the method of Dollimore and Heal (22) from the desorption branch of the adsorption–desorption isotherm of nitrogen at −196°C.

Ni metal surface areas of the reduced samples were determined by hydrogen chemisorption at 0°C in a conventional volumetric gas adsorption apparatus. Prior to the measurement, the catalyst sample was reduced by hydrogen under an initial pressure of 39.5 kPa at 500°C for 2 h, and then the sample was outgassed under vacuum for 1 h at the same temperature to remove hydrogen adsorbed on the catalyst. Hydrogen uptakes were measured at 6.6, 13.2, and 26.6 kPa, and the amount of chemisorbed H_2 was calculated by the Langmuir adsorption equation for the H_2 uptake data. The nickel surface area was calculated from the amount of chemisorbed H_2, assuming that chemisorption stoichiometry was H/Ni = 1 and the Ni surface area was occupied by hydrogen atoms equaling 0.065 nm^2 (23).

For Raney Ni catalysts, after the samples washed with hexane had been outgassed at 50°C for 1 h without further reduction, they served for the adsorption of nitrogen and hydrogen.

Catalytic Reaction

Hydrogenations of cyclohexanone, acetone, 2-butanone, 3-pentanone, and 4-heptanone were tested in the following procedure. A mixed solution (10 cm^3) of a reactant ketone (9.6 mmol) and a solvent hexane was added to the glass vessel with the freshly prepared Ni catalyst under hydrogen flow conditions. The hydrogenation was performed in a stirred pressure batch reactor (Taiatsu Tecno Co., TVS-1). After the reactor had been cooled to the reaction temperature of 0°C, the inside of the reactor was purged with hydrogen three times. Supplying hydrogen at a pressure of 1.1 MPa started the catalytic reaction. During the hydrogenation, the pressure was kept at 1.1 MPa, and the solution was stirred at a stirring speed of 1350 rpm. After 5–30 min had elapsed, reducing the pressure to 0.1 MPa stopped the reaction. The reaction mixture filtered with a glass filter was analyzed by FID-GC with a fused silica capillary column of TC-WAX (30 m) at 30°C.

Analysis of Reaction Rate Data

The reaction rate of the catalysts was calculated from the conversion of ketone to the corresponding secondary alcohol. The conversion data were fitted to the integral form of first-order rate, $kt = \ln[1/(1-X)]$, where k, t, and X are the first-order reaction rate constant, process time, and conversion of ketone, respectively [p. 62 in Ref. (18)]. Then, the rate constant, k, was divided by the catalyst weight used to obtain the first-order rate constants per unit weight of catalyst, k_w. The turnover frequency, TOF, is defined as

the number of molecules reacted per surface Ni atom per minute.

Since the NiO–MgO precursors consisted of complete solid solutions of NaCl-type crystal structure (11), we can assume that the distribution of Ni metal surface exposed on the catalyst surface is also proportional to the pore size distribution of the Ni–MgO catalyst after reduction of NiO–MgO as well as Raney Ni catalysts. The cumulative Ni surface area of the catalyst was estimated by integrating the Ni surface areas in pores larger than a definite pore size, as shown in Fig. 7 for typical samples. Then, the best colinearity between the cumulative Ni surface area and the reaction rate constant (k_w) was calculated by using a least-squares method for linear approximation; an example is shown in Fig. 8. At the pore size that provided the highest correlation coefficient (r) between cumulative Ni surface area and k_w, we judged that the surface reaction is slower than mass diffusion. In pores smaller than this size, however, it is interpreted that diffusion is predominant.

RESULTS

We preliminarily examined the effect of stirring speed in the batch reactor on eliminating interparticle mass-transfer resistance. Figure 1 shows the effect of stirring speed on the conversion of 4-heptanone. The conversion was constant at stirring speeds higher than 1200 rpm. This indicates that interparticle diffusion is removed by agitation above 1200 rpm. Thus, we examined the following catalytic tests at a stirring speed of 1350 rpm. Then, we evaluated the reaction order for the reactant ketone. Figure 2 shows ln[1/(1−X)]-versus-process time plots for typical samples in the hydrogenation of cyclohexanone, where X is the cyclohexanone conversion. The linear correlation indicates that the hydrogenation is first order of reactant cyclohexanone.

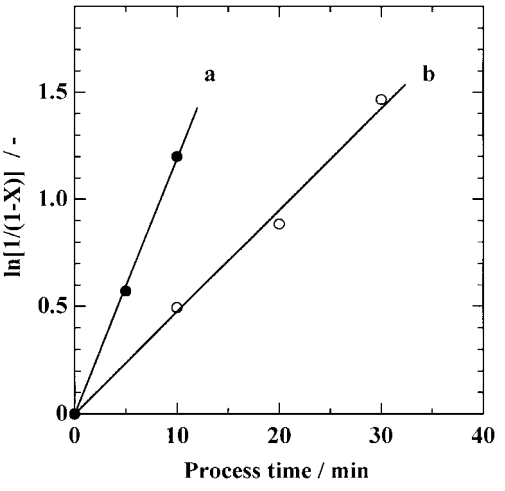

FIG. 2. Ln[1/(1−X)]-versus-time plot for typical catalyst samples. The hydrogenation of cyclohexanone was done at 0°C at a hydrogen pressure of 1.1 MPa, and the solution (10 cm^3) containing cyclohexanone (9.6 mmol) was stirred at a stirring rate of 1350 rpm using (a) Ni(70 wt%)–MgO reduced at 500°C after calcination at 400°C and (b) Raney 40.

Figure 3 shows the variations in the first-order rate constant (k_w) for the hydrogenation of cyclohexanone and in Ni surface area of Ni–MgO catalyst with calcination temperature of NiO–MgO precursors. Even if the reduction conditions were fixed at 500°C for 2 h, both k_w and Ni surface area varied with the prior calcination temperature. Ni–MgO exhibited a maximum rate constant at a calcination temperature of 400°C. The Ni surface area monotonously decreased with increasing calcination temperature, in contrast to showing the maximum in the catalytic hydrogenation. Table 1 lists the data together with specific surface

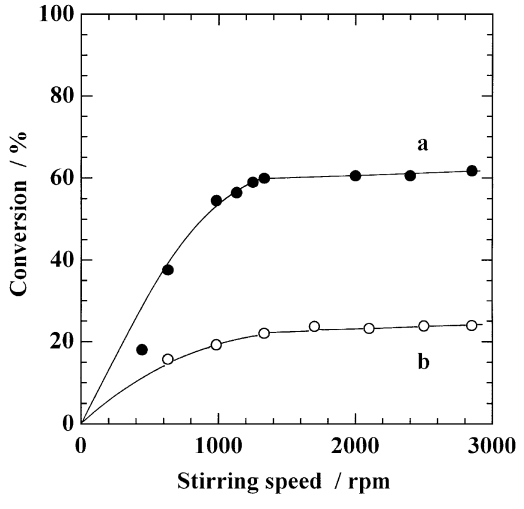

FIG. 1. Effect of stirring speed on the conversion of 4-heptanone. The solution (10 cm^3) containing 4-heptanone (9.6 mmol) was reacted at 0°C for 30 min at a hydrogen pressure of 1.1 MPa using (a) Ni(70 wt%)–MgO calcined at 500°C and (b) Raney 50.

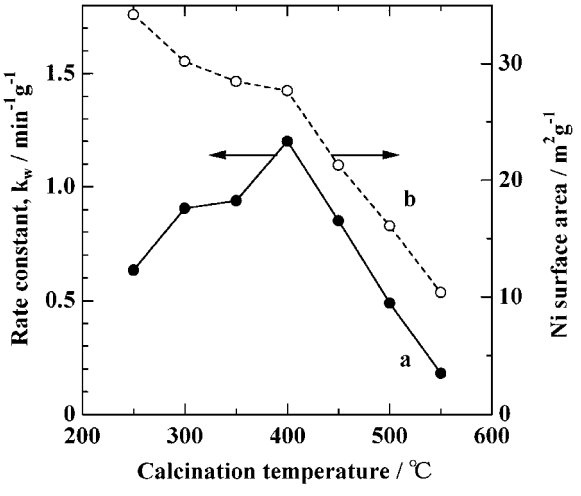

FIG. 3. Variations in (a) the first-order rate constant for the hydrogenation of cyclohexanone and (b) Ni surface area with calcination temperature.

TABLE 1

Physical and Catalytic Properties of Ni(70 wt%)–MgO

Calcination (°C)	Total SA[a] ($m^2\ g^{-1}$)	Ni SA[b] ($m^2\ g^{-1}$)	k_w[c] ($min^{-1}\ g^{-1}$)	TOF[d] (min^{-1})
250	95	34.2	0.63	6.8
300	94	30.2	0.91	11.2
350	96	28.5	0.94	12.4
400	93	27.7	1.20	16.2
450	89	21.3	0.85	15.0
500	56	16.1	0.49	11.2
550	49	10.4	0.18	6.4

[a] Total surface area of the sample reduced at 500°C for 2 h, measured by N_2 adsorption at −196°C.

[b] Ni surface area calculated from the amount of H_2 adsorbed on the reduced sample.

[c] First-order rate constant per unit weight of catalyst; the hydrogenation of cyclohexanone was done at 0°C at a hydrogen pressure of 1.1 MPa, and the solution (10 cm^3) containing cyclohexanone (9.6 mmol) was stirred at a stirring rate of 1350 rpm.

[d] TOF is calculated with the equation $TOF = k_w \times (0.065\ nm^2) \times (0.0096\ mol) \times (6.02 \times 10^{23})/(Ni\ SA \times 10^{18}\ nm^2\ g^{-1})$.

area and TOF. There was no simple correlation between reaction rate data (k_w and TOF) and Ni surface area.

Figure 4 shows the variations in the first-order rate constant (k_w) for the hydrogenation of cyclohexanone with Ni content. Two series of catalysts calcined at different temperatures, 400°C (curve a) and 500°C [curve b, data were taken from Table 1 in Ref. (12)], were examined. For both calcination temperatures, the reaction rate constants were maximized at a Ni content of 70 wt%. The Ni–MgO catalysts calcined at 400°C were more active than those calcined at 500°C. Moreover, when NiO–MgO had been calcined at 400°C, Ni–MgO catalysts with 60–80 wt% Ni were more active than the reference Raney 40 and 50 catalysts (plots c and d in Fig. 4).

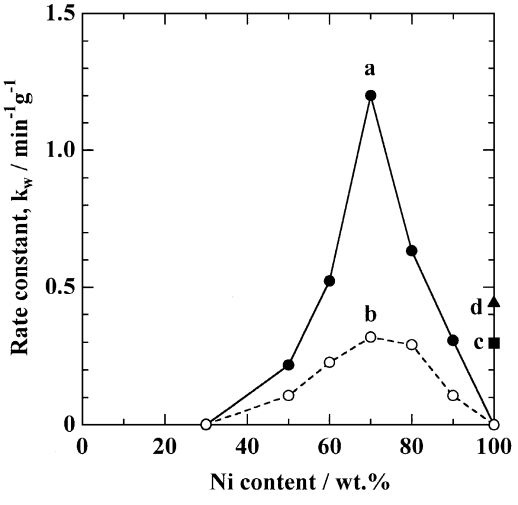

FIG. 4. Variations in the first-order rate constant for the hydrogenation of cyclohexanone with Ni content. (a) Ni–MgO calcined at 400°C; (b) Ni–MgO calcined at 500°C [data were taken from Table 1 in Ref. (12)]; (c) Raney 50; (d) Raney 40.

Table 2 summarizes the reaction rate data (k_w and TOF), specific surface area, and Ni surface area of Ni–MgO samples calcined at 400°C together with those of reference Raney Ni catalysts. The specific surface area of the Ni–MgO samples decreased monotonously with increasing Ni content (second column in Table 2). On the other hand, Ni metal surface area showed a maximum of 28.2 $m^2\ g^{-1}$ at a Ni content of 80 wt%. Although the values are larger than those of 500°C-calcined samples, the variations of these characteristics are similar to the variations of those calcined at 500°C (12). In addition, the reference Raney 40 and 50 catalysts had large Ni surface areas of 41.5 and 37.0 $m^2\ g^{-1}$, respectively, while they had reaction rates smaller than those of Ni–MgO catalysts. There was also a significant difference among the TOF values in the various porous Ni catalysts, as noted in Table 1.

Figures 5 and 6 depict the pore size distributions of several Ni catalysts. Pore sizes of Ni(70 wt%)–MgO were shifted to larger size with increasing calcination temperature (Fig. 5). Compared with the Raney Ni catalysts, the Ni(70 wt%)–MgO catalyst had large pores (Fig. 6). The Ni(70 wt%)–MgO catalyst mainly had mesopores at radii around 2–4 nm, while the Raney Ni catalyst had pores smaller than 2 nm. Raney Ni catalysts with different Ni–Al alloy compositions had also different pore size distributions: Raney 40 had pores larger than those of Raney 50 (Fig. 6). The cumulative Ni surface area of the catalyst was calculated by multiplying Ni surface area by pore size distribution. Cumulative Ni surface areas of typical samples are depicted in Fig. 7.

Figure 8 shows the relationship between Ni metal surface area and the first-order rate constant for the hydrogenation

TABLE 2

Physical and Catalytic Properties of Ni–MgO Samples

Ni content (wt%)	Total SA[a] ($m^2\ g^{-1}$)	Ni SA[b] ($m^2\ g^{-1}$)	k_w[c] ($min^{-1}\ g^{-1}$)	TOF[d] (min^{-1})
NiO–MgO calcined at 400°C				
30	120	4.2	0	0
50	110	13.3	0.22	6.4
60	101	18.6	0.52	10.5
70	93	27.7	1.20	16.2
80	70	28.2	0.63	8.3
90	54	18.8	0.31	6.0
100	20	0.1	0	0
Raney Ni				
100[e]	102	41.5	0.44	0.6
100[f]	116	37.0	0.30	1.6

[a–d] See Table 1.

[e] Raney 40.

[f] Raney 50.

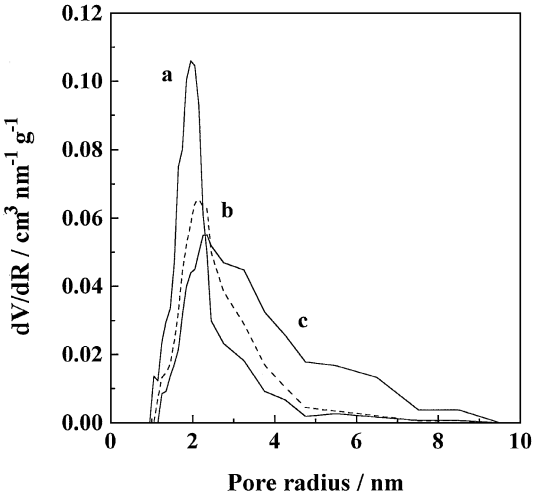

FIG. 5. Pore size distributions of various Ni–MgO catalysts. The samples were reduced with H_2 at 500°C for 2 h prior to the measurement. (a) Ni(70 wt%)–MgO calcined at 250°C; (b) Ni(70 wt%)–MgO calcined at 350°C; (c) Ni(70 wt%)–MgO calcined at 450°C.

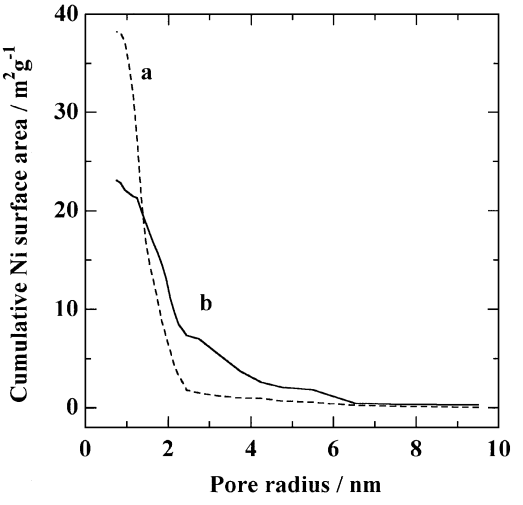

FIG. 7. Variations in the cumulative Ni surface areas of Raney Ni and Ni–MgO. (a) Raney 50; (b) Ni(70 wt%)–MgO calcined at 450°C.

of cyclohexanone. The first-order rate constants were plotted against total Ni surface area (Fig. 8a); they had no correlation with total Ni surface area. The rate constant, however, is found to be proportional to cumulative Ni surface area in pores larger than 2.3 nm in radius (Fig. 8b). In other words, the best colinearity between the cumulative Ni surface area and k_w has been obtained at a pore radius of 2.3 nm for the hydrogenation of cyclohexanone. Then, in a least-squares method for linear approximation, a correlation coefficient (r) between a cumulative Ni surface area and k_w was estimated for each pore radius. Figure 9 shows the change in correlation coefficient (r) for the hydrogenation of cyclohexanone with pore radius. Definitely, the highest value of r was obtained at a pore radius of 2.3 nm.

For other reactants, Figs. 10–13 show the relationship between Ni surface area and k_w for the hydrogenation of several ketones. For the hydrogenation of acetone to 2-propanol (Fig. 10), k_w was directly proportional to total Ni surface area. In contrast, for the hydrogenation of 2-butanone, 3-pentanone, and 4-heptanone (Figs. 11a, 12a,

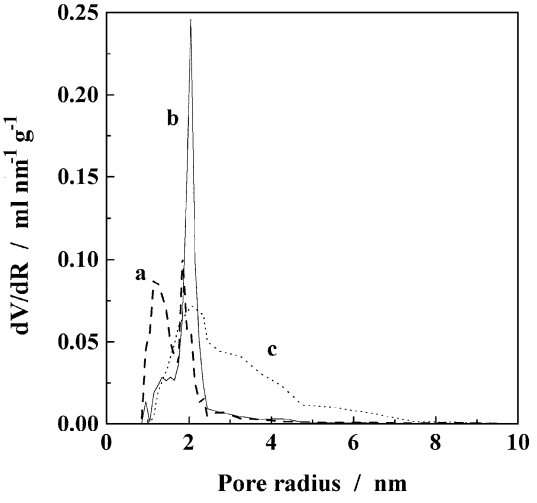

FIG. 6. Comparison of pore size distributions between Raney Ni and Ni–MgO catalysts. Curve a, Raney 50; b, Raney 40; c, Ni(70 wt%)–MgO calcined at 400°C.

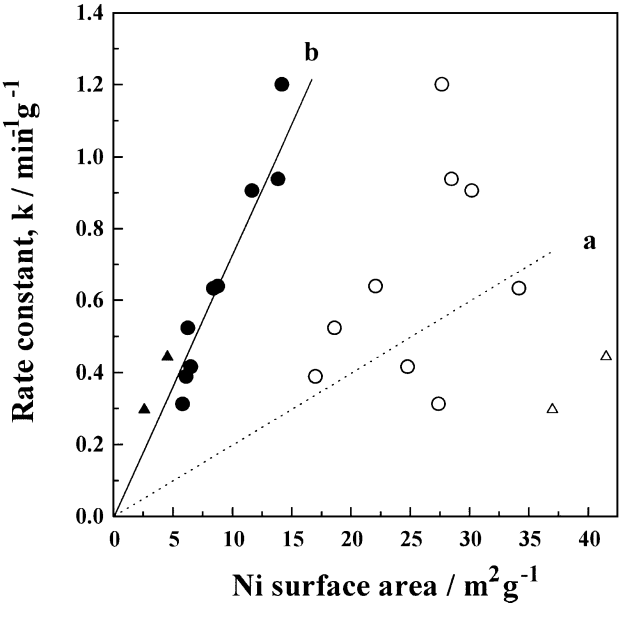

FIG. 8. Relationship between Ni surface area and the first-order rate constant for the hydrogenation of cyclohexanone. Open symbols (a) represent total Ni surface area, and closed symbols (b), the Ni surface area in pores larger than 2.3 nm in radius. Circles represent Ni–MgO catalysts, and triangles, Raney Ni catalysts.

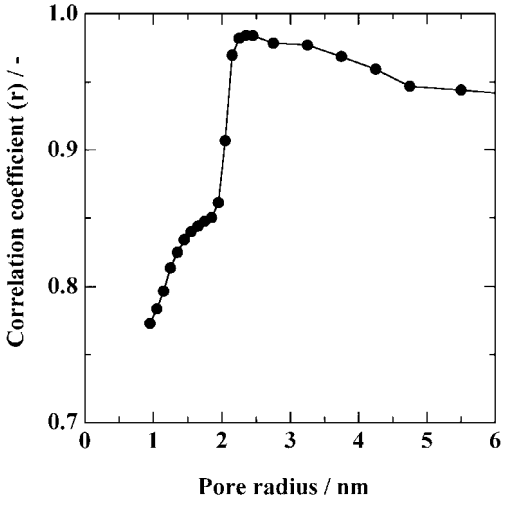

FIG. 9. Change in correlation coefficient in the linear approximation for the relation between the rate constant and Ni surface area with different pore radii for the hydrogenation of cyclohexanone.

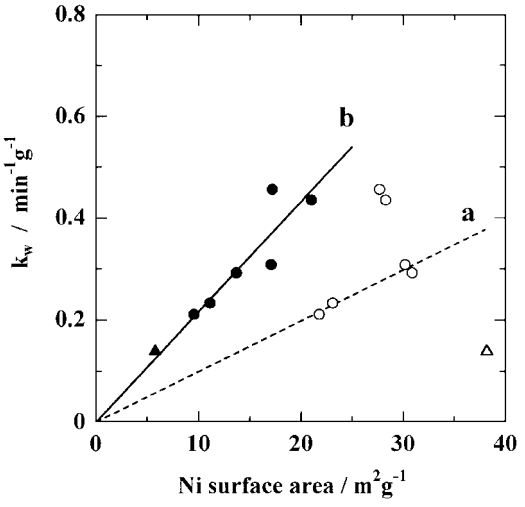

FIG. 11. Relationship between Ni surface area and the rate constant for the hydrogenation of 2-butanone. Open symbols (a) represent total Ni surface area, and closed symbols (b), the Ni surface area in pores larger than 2.0 nm in radius. Circles represent Ni–MgO catalysts, and triangles, Raney 50.

and 13a, respectively), the rate constants had no definite correlation with total Ni surface area. We then, tried to show variations in correlation coefficients with pore radius, as was shown for the hydrogenation of cyclohexanone in Fig. 9. Figure 14 depicts the changes in correlation coefficients for the hydrogenations of acetone, 2-butanone, 3-pentanone, and 4-heptanone. The correlation coefficients were highest at pore radii of 1.1, 2.0, 3.2, and 3.7 nm for acetone, 2-butanone, 3-pentanone, and 4-heptanone, respectively. At the critical pore radii, the rate constant was found to be proportional to the cumulative Ni surface area for each reactant (Figs. 11b, 12b, and 13b).

Figure 15 summarizes the linear correlations between k_w and cumulative Ni surface area for the five reactants mentioned above. There were differences in the catalytic reactivities among the reactants. They were classified into three groups: acetone and 2-butanone (Fig. 15a), 3-pentanone and cyclohexanone (Fig. 15b), and 4-heptanone (Fig. 15c). The hydrogenation rates of 3-pentanone and cyclohexanone were fastest, and those of acetone and 2-butanone were faster than that of 4-heptanone.

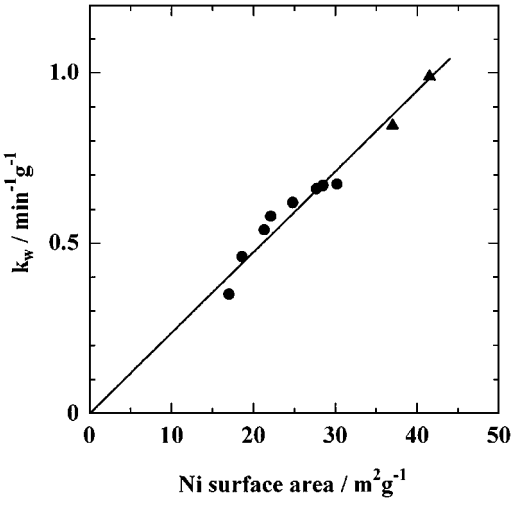

FIG. 10. Relationship between total Ni surface area and the rate constant for the hydrogenation of acetone. Circles represent Ni–MgO catalysts, and triangles, Raney 40 and 50.

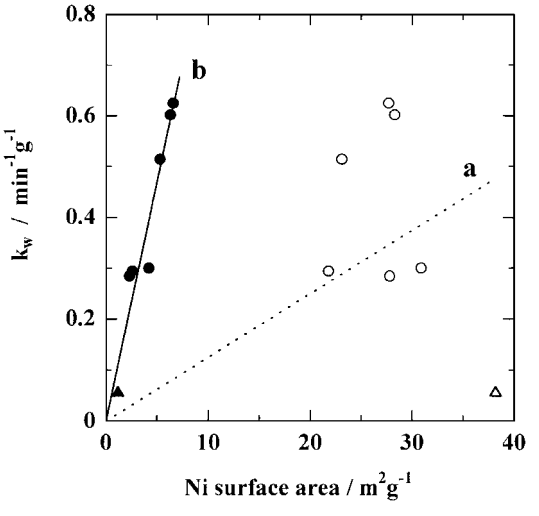

FIG. 12. Relationship between Ni surface area and the rate constant for the hydrogenation of 3-pentanone. Open symbols (a) represent total Ni surface area, and closed symbols (b), the Ni surface area in pores larger than 3.2 nm in radius. Circles represent Ni–MgO catalysts, and triangles, Raney 50.

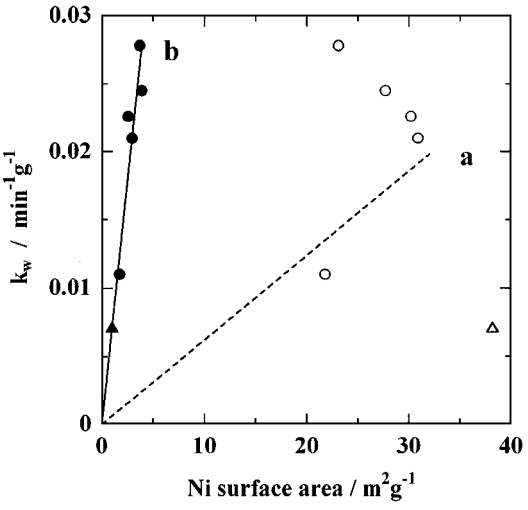

FIG. 13. Relationship between Ni surface area and the rate constant for the hydrogenation of 4-heptanone. Open symbols (a) represent total Ni surface area, and closed symbols (b), the Ni surface area in pores larger than 3.7 nm in radius. Circles represent Ni–MgO catalysts, and triangles, Raney 50.

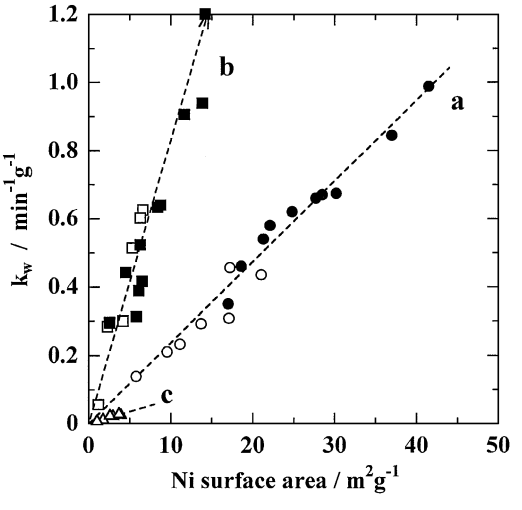

FIG. 15. Comparison of the rate constants among the five reactants. (a) ●, Acetone; ○, 2-butanone. (b) ■, cyclohexanone; □, 3-pentanone. (c) △, 4-heptanone.

DISCUSSION

Hydrogenation over Ni–MgO with High Ni Surface Area

We previously reported that Ni–MgO with a Ni content of 70 wt%, which was obtained by calcining an amorphous mixture of citrate at 500°C and following reduction at 500°C, had a Ni surface area as high as 20 m^2 g^{-1} (10–12). In this report, we found that Ni surface area increased with decreasing calcination temperature of the amorphous mixture of citrate (Fig. 3b). The Ni surface area of Ni–MgO reached 30 m^2 g^{-1} after calcination at 300°C. Thus, we can demonstrate that high Ni surface area is realized by using precursor samples calcined at the lower temperatures.

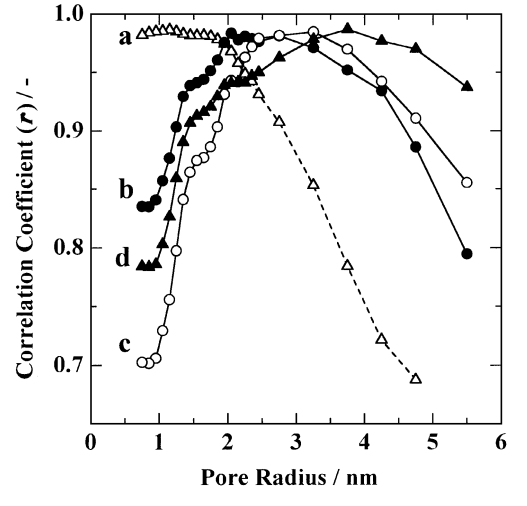

FIG. 14. Change in correlation coefficient (r) in the linear approximation for the relation between the first-order rate constant and Ni surface area with different pore radii for the hydrogenation. (a) Acetone; (b) 2-butanone; (c) 3-pentanone; (d) 4-heptanone.

The reference commercial Raney Ni samples (Raney 40 and 50) had large Ni surface areas of 41.5 and 37.0 m^2 g^{-1}, respectively (Table 2). The values were smaller than those reported previously (12), probably because of the difference in Al leaching conditions. The physical properties of Raney Ni such as Ni surface area and pore structure vary widely with conditions of leaching Al from Ni–Al alloy (13, 21, 24). In particular, the Ni surface area of Raney Ni catalyst varies with the Al leaching temperature (13).

Although the Ni surface areas of the Ni–MgO catalysts were smaller than those of the Raney Ni catalysts, the Ni–MgO catalysts had large k_w values (Table 2). Especially at a calcination temperature of 400°C, Ni–MgO of high Ni content ranging from 60 to 80 wt% had an excellent reaction rate for the liquid-phase hydrogenation of cyclohexanone (Fig. 4). However, there is no correlation between k_w and Ni surface area of the catalyst (Fig. 8a). In the literature (13), it has also been reported that catalytic activities sometimes have no correlation with Ni metal surface area for Raney Ni catalysts. Thus, we speculated that the significant difference in TOF values among the catalysts depended on either the chemical effect of the MgO additive on catalytic activity of Ni or the physical effect of diffusion of the reactants in mesopores of the catalyst (12).

The chemical effect is considered as follows: residual Al in the Raney Ni catalyst may decrease the hydrogenation activity of Ni; in contrast, MgO in the Ni–MgO catalyst may accelerate catalytic activity. For Raney Ni catalysts, furthermore, residual hydrogen after leaching Al from Ni–Al alloy has been speculated to involve catalytic hydrogenation

(25, 26). This kind of chemical effect cannot be expressed quantitatively. In the vapor phase, on the other hand, reaction rates in hydrogenolysis and hydrogenation are roughly proportional to the Ni surface area of the Ni–MgO samples (10, 11). Although we do not deny the existence of residual hydrogen in Raney Ni, we do not think that additive MgO in Ni–MgO catalyst accelerates the hydrogenation rate. Unfortunately, the chemical effect of MgO on catalytic activity has still not been clarified. Since we speculate that the significant difference among the TOF values in Tables 1 and 2 depends on the diffusivity of reactants in the catalyst pores (19), we intend to discuss this point in the following section.

Diffusion Limitation in Mesopore of Catalyst

In general, mass transfer of H_2 in liquid phase is faster than that of organic reactants (16). Notheisz *et al.* examined a mass-transfer test during liquid-phase hydrogenation of cyclohexene catalyzed by silica-supported Pd and Pt (27). They found that the stirring speed was concerned with mass transfer; the gas-to-liquid mass-transfer resistance was negligible compared with other resistance at ambient temperature above 1550 rpm. In this work, because the rate constant, k_w, was independent of the stirring speed above 1200 rpm (Fig. 1), we carried out the hydrogenation tests at a stirring speed of 1350 rpm.

We have previously demonstrated the comparison of pore size distributions of Ni–MgO catalyst and Raney Ni catalyst [Figs. 2 and 3 in Ref. (12)], in a similar manner as in Fig. 6. In the previous report (12), we calculated the pore size distribution with the method reported by Cranston and Inkley (28). In this report, we employed a calculation method proposed by Dollimore and Heal (23) because this method can provide desirable intervals of pore radius in the calculation of pore size distribution. The shift in pore size distribution of Ni–MgO to larger size with increasing calcination temperature (Fig. 5) is opposite that observed in pure MgO (29). Since the reduction of NiO–MgO at 500°C does not affect the pore size distribution, NiO-rich catalysts follow a different trend with pure MgO. At either calcination temperature of 400 or 500°C, the Ni(70 wt%)–MgO catalysts have mesopores larger than those in the Raney Ni catalysts.

For the NiO–MgO binary system, both end members have NaCl-type crystal structure, and a complete series of solid solution occurs. NiO–MgO solid solution is readily obtained by calcining the amorphous citrate mixtures (11). In the solid solution, MgO possibly acts as an obstacle preventing the aggregation of nickel oxide, because the specific surface area decreases monotonously with increasing NiO content. This is a typical example of the formation of a complete solid solution through the citrate process, whereas other combinations such as CeO_2–MgO (30) and CuO–Al_2O_3 (31) form a partial solid solution and a spinel-type compound of $CuAl_2O_4$, respectively. Since it is considered that the Ni component is highly dispersed on the NiO–MgO solid solution, reduced Ni particles on the NiO–MgO solid solution are possibly distributed in the mesopores of catalyst with uniform concentration. Thus, it is also assumed that the Ni surface after reduction is distributed with uniform concentration in the mesopores of Ni–MgO catalyst as well as Raney Ni. Therefore, the data processing shown in Fig. 7 is said to be reasonable.

Then, we tried to explain why the rate constant (k_w) is not proportional to Ni surface area by using mass-transfer limitation in the mesopore of catalysts. If the liquid-phase hydrogenation in pores of smaller size is limited by the diffusion step of reactants and/or products, the Ni surface in the small pores must not directly affect reaction rate.

A linear correlation has been observed between total Ni surface area and k_w only for the acetone hydrogenation (Fig. 10). For the other hydrogenations except that of acetone, no simple correlation between Ni surface areas and k_w is observed (Figs. 8a, 11a, 12a, and 13a). As shown in Figs. 8b and 9, for the hydrogenation of cyclohexanone, k_w is approximately proportional to Ni metal surface area in pores larger than 2.3 nm in radius. This indicates that the Ni surface in pores larger than the critical size of 2.3 nm in radius plays an effective role in the hydrogenation of cyclohexanone. In other words, mass transfer of reactants and/or products is strongly restricted in pores smaller than 2.3 nm. Figure 14 also indicates that mass transfer of reactants such as acetone, 2-butanone, 3-pentanone, and 4-heptanone is restricted in pores smaller than 1.1, 2.0, 3.2, and 3.7 nm in radius, respectively. Although Fig. 10 indicates that acetone hydrogenation is not affected by pore diffusion, the best colinearity is obtained at a radius of 1.1. The sizes are assumed to be minimum radii through which the reactants can move with negligible mass-transfer resistance in the catalyst pores; the mass-transfer resistance in pores smaller than the critical radius is larger than the resistance of the surface reaction including hydrogenation and adsorption of ketone. Thus, we suppose that mass transfer rate in pores smaller than the critical pore size decreases to some lower rate rather than zero.

As shown in Fig. 15, Ni catalysts show different catalytic activities among several ketones; the hydrogenations of 3-pentanone and cyclohexanone were the fastest of the five reactants, and those of acetone and 2-butanone are faster than that of 4-heptanone. The ring of cyclohexanone is so strained that the hydrogenation may be faster than those of the other reactants. However, the reason why the hydrogenation of 3-pentanone is so fast and the hydrogenation of 4-heptanone is so slow is not clear. It may be temporarily speculated that it is based on differences in the adsorption rates of reactants on the Ni surface, the solvation of reactant, and so on. Further investigation is needed to solve the question.

Relation between Reactant Size and Mass-Transfer Limitation

The rate constants for the hydrogenation of several ketones are found to be proportional to the cumulative Ni surface areas in pores larger than the critical sizes. In the liquid-phase hydrogenation under a pressure of 1.1 MPa at 0°C, the critical pore sizes depend on the sizes of reactant: movement of acetone, 2-butanone, cyclohexanone, 3-pentanone, and 4-heptanone is restricted in pores smaller than 1.1, 2.0, 2.3, 3.2, and 3.7 nm in radius, respectively (Figs. 9 and 14). We then attempted to elucidate a relation between reactant molecule size and critical pore size.

Several factors such as length and cross section of reactant molecules had been used for the trial, but no clear relation was obtained. The inverse volume of a molecule, i.e., number of molecules in unit volume (N_m), however, provided a linear relation with critical radius (R_{cp}), which indicated the minimum pore radius releasing from mass-transfer limitation (Fig. 16). The N_m value was calculated from density of reactant, molecular weight, and Avogadro's number; the data are also listed in Table 3. From the line shown in Fig. 16, the following equation was obtained:

$$R_{cp} = 6.72 - 0.70N_m. \quad [1]$$

Because the numerical values of N_m are calculated from the density of pure reactant, actual values of the reactants might be somewhat different in the hexane solution used in this work. The critical pore size is 10 times as large as molecule size, i.e., diameter and length. This equation means that the volume of reactant restricts the mobility of reactant molecule in a solvent.

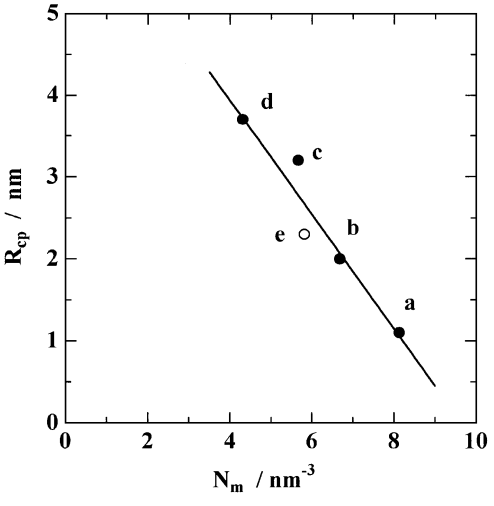

FIG. 16. Relationship between numbers of molecules in unit volume (N_m) and critical pore radius (R_{cp}). (a) Acetone; (b) 2-butanone; (c) 3-pentanone; (d) 4-heptanone; (e) cyclohexanone. The R_{cp} values were estimated from in Figs. 9 and 14.

TABLE 3

Physical Data on Reactants and R_{cp}

Reactant	Molecular weight[a] (g mol^{-1})	Density[a] (g cm^{-3})	N_m[b] (nm^{-3})	R_{cp}[c] (nm)	r[d]
Acetone	58.08	0.7845[e]	8.13	1.1	0.986
2-Butanone	72.11	0.7999[e]	6.68	2.0	0.983
Cyclohexanone	98.14	0.9478[f]	5.81	2.3	0.984
3-Pentanone	86.13	0.8098[e]	5.66	3.2	0.984
4-Heptanone	114.19	0.8174[f]	4.31	3.7	0.987

[a] Data are referenced in Ref. (32).
[b] Number of molecules in unit volume calculated density of reactant (g cm^{-3}), molecular weight (g mol^{-1}), and Avogadro's number (mol^{-1}); N_m = (density of reactant $\times 10^{-21}$) $\times$ (6.02×10^{23})/(molecular weight).
[c] Critical radius; data obtained from Figs. 9 and 14.
[d] r is the maximum correlation coefficient that provides R_{cp}.
[e] At 25°C.
[f] At 20°C.

It is reported that reaction rates varied with reactants, such as cyclohexene, cyclohexanone, benzene, and phenol, in comparison to Raney Ni catalysts (25), when reacted under different reaction conditions: reaction temperature and pressure of H_2. However, there was no discussion of the mass-transfer limitation (25). Although we need further data under different reaction conditions (pressure, temperature, solvent etc.), Eq. [1] can provide an expression of mass-transfer limitation in mesopores in hexane solvent under a pressure of 1.1 MPa at 0°C. In this report, we state only that the correlation between R_{cp} and N_m has been experimentally arranged by the simple equation (Eq. [1]). The physico-chemical meaning of Eq. [1] is still unclear and remains for future study.

CONCLUSION

The liquid-phase hydrogenation of cyclohexanone, acetone, 2-butanone, 3-pentanone, and 4-heptanone to the corresponding secondary alcohols was examined over various porous Ni catalysts under a hydrogen pressure of 1.1 MPa at 0°C. Pore size distributions as well as Ni surface area of Ni–MgO catalysts, which were prepared from a melt of the corresponding nitrates and citric acid, with high Ni contents of 60–80 wt% were found to be controlled by the calcination temperatures of the precursors.

For acetone hydrogenation, first-order reaction rate constants were proportional to Ni surface area of the catalyst, and Raney nickel with the largest Ni surface area showed the highest reaction rate constant. For the hydrogenation of the other reactants larger than acetone, however, rate constants did not have a simple linear relation with Ni surface area. The Ni-MgO catalysts with large mesopores exceeded Raney Ni catalysts.

We estimated the degree of contribution of Ni in small pores to the liquid-phase hydrogenation by analyzing the

reaction rate data coupled with pore size distribution and Ni surface area. Cumulative Ni surface areas were calculated by multiplying the Ni surface area by a fraction of cumulative surface area located in pores larger than a specific size to the total surface area, and relationship between the cumulative Ni surface areas and the rate constants were examined. The rate constants for the hydrogenation of 2-butanone, 3-pentanone, and 4-heptanone are approximately proportional to the cumulative Ni surface areas in pores larger than the critical sizes. The critical size was found to depend on the size of the reactant: the diffusion of acetone, 2-butanone, cyclohexanone, 3-pentanone, and 4-heptanone was restricted in pores smaller than 1.1, 2.0, 2.3, 3.2, and 3.7 nm in radius, respectively.

REFERENCES

1. Rylander, P. N., "Catalytic Hydrogenation in Organic Syntheses," p. 82. Academic Press, New York, 1979.
2. Lieber, E., and Morritz, F. L., *Adv. Catal.* **5**, 266 (1953).
3. Mikhailenko, S. D., Fasman, A. B., Maksimova, N. A., and Leongard, E. V., *Appl. Catal.* **12**, 141 (1984).
4. Imamura, H., Kato, Y., Yamada, K., and Tsuchiya, S., *Appl. Catal.* **27**, 243 (1986).
5. Bonnier, J. M., Damon, J. P., and Masson, J., *Appl. Catal.* **30**, 181 (1987).
6. Masson, J., Vedal, S., Cividino, P., Fouiloux, P., and Court, J., *Appl. Catal. A* **99**, 147 (1993).
7. Chen, A. S. C., Chen, C., and Lin, Y., *Appl. Catal. A* **119**, L1 (1994).
8. Brown, C. A., *J. Org. Chem.* **35**, 1900 (1970).
9. Wang, H., Yu, Z., Chen, H., Yang, J., and Deng, J., *Appl. Catal. A* **129**, L143 (1995).
10. Sato, S., Nozaki, F., and Nakayama, T., *Appl. Catal. A* **139**, L1 (1996).
11. Nakayama, T., Ichikuni, N., Sato, S., and Nozaki, F., *Appl. Catal. A* **158**, 185 (1997).
12. Nakayama, T., Yamashiro, K., Sato, S., and Nozaki, F., *Appl. Catal. A* **151**, 437 (1997).
13. Freel, J., Pieters, W. J. M., and Anderson, R. B., *J. Catal.* **18**, 243 (1970).
14. Riekert, L., *Adv. Catal.* **21**, 281 (1970).
15. Bhatia, S., "Zeolite Catalysis: Principles and Applications," p. 49. CRC Press, Boca Raton, FL, 1989.
16. Boudart, M., and Cheng, W.-C., *J. Catal.* **106**, 134 (1987).
17. Rylander, P. N., "Catalytic Hydrogenation in Organic Syntheses," p. 1. Academic Press, New York, 1979.
18. Smith, J. M., "Chemical Engineering Kinetics," 3rd. ed., p. 450. McGraw–Hill, New York, 1981.
19. Madon, R. J., and Boudart, M., *Ind. Eng. Chem. Fundam.* **21**, 438 (1982).
20. Kokubomatsu, T., and Komatsu, S., "Raney Catalyst," p. 42. Kyoritsu, Tokyo, 1971. [In Japanese]
21. Freel, J., Pieters, W. J. M., and Anderson, R. B., *J. Catal.* **14**, 247 (1969).
22. Dollimore, D., and Heal, G. R., *J. Appl. Chem.* **14**, 109 (1964).
23. Bartholomew, C. H., and Farrauto, R. J., *J. Catal.* **45**, 41 (1976).
24. Wainright, M. S., and Anderson, R. B., *J. Catal.* **64**, 124 (1980).
25. Nishimura, S., Kawashima, M., Inoue, S., Takeoka, S., and Shimizu, M., *Appl. Catal.* **76**, 19 (1991).
26. Hochard, F., Jobic, H., Massardier, J., and Renouprez, A. J., *J. Mol. Catal.* **95**, 165 (1995).
27. Notheisz, F., Zsigmond, A., Bartok, M., Szegletes, Z., and Smith, G. V., *Appl. Catal. A* **120**, 105 (1994).
28. Cranston, R. W., and Inkley, F. A., *Adv. Catal.* **9**, 143 (1957).
29. Nakayama, T., Sato, S., and Nozaki, F., *Bull. Chem. Soc. Jpn.* **69**, 2107 (1996).
30. Sato, S., Koizumi, K., and Nozaki, F., *J. Catal.* **178**, 264 (1998).
31. Sato, S., Iijima, M., Nakayama, T., Sodesawa, T., and Nozaki, F., *J. Catal.* **169**, 447 (1997).
32. Lide, D. R. (Ed.), "Handbook of Chemistry and Physics," 79th ed. CRC Press, Boca Raton, FL, 1998.